

**This is a self-archived version of an original article. This version may differ from the original in pagination and typographic details.**

**Author(s):** Alayyaf, Abdulmajeed Abdullah; Barakat, Assem; Al-Majid, Abdullah Mohammed; Ali, M.; Yousuf, Sammer; Haukka, Matti; El-Faham, Ayman; Soliman, Saied M.; Nafie, Mohamed S.

**Title:** Cytotoxicity and Apoptosis-Induction in MCF-7 Cells for New Pd(II) Complex Based on s-Triazine Ligand : Synthesis, Single Crystal X-ray Diffraction Analysis and Structural Investigations

**Year:** 2023

**Version:** Published version

**Copyright:** © 2023 by the authors. Licensee MDPI, Basel, Switzerland

**Rights:** CC BY 4.0








**Rights url:** <https://creativecommons.org/licenses/by/4.0/>

**Please cite the original version:**

Alayyaf, A. A., Barakat, A., Al-Majid, A. M., Ali, M., Yousuf, S., Haukka, M., El-Faham, A., Soliman, S. M., & Nafie, M. S. (2023). Cytotoxicity and Apoptosis-Induction in MCF-7 Cells for New Pd(II) Complex Based on s-Triazine Ligand : Synthesis, Single Crystal X-ray Diffraction Analysis and Structural Investigations. *Crystals*, 13(10), Article 1472. <https://doi.org/10.3390/cryst13101472>

## Article

# Cytotoxicity and Apoptosis-Induction in MCF-7 Cells for New Pd(II) Complex Based on *s*-Triazine Ligand: Synthesis, Single Crystal X-ray Diffraction Analysis and Structural Investigations

Abdulmajeed Abdullah Alayyaf <sup>1</sup>, Assem Barakat <sup>1,\*</sup>, Abdullah Mohammed Al-Majid <sup>1</sup>, M. Ali <sup>1</sup>, Sammer Yousuf <sup>2</sup>, Matti Haukka <sup>3</sup>, Ayman El-Faham <sup>4</sup>, Saied M. Soliman <sup>4</sup> and Mohamed S. Nafie <sup>5,6</sup>

<sup>1</sup> Department of Chemistry, College of Science, King Saud University, P.O. Box 2455, Riyadh 11451, Saudi Arabia; mayyaf@ksu.edu.sa (A.A.A.); amajid@ksu.edu.sa (A.M.A.-M.); maly.c@ksu.edu.sa (M.A.)

<sup>2</sup> H.E.J. Research Institute of Chemistry, International Center for Chemical and Biological Sciences, University of Karachi, Karachi 75270, Pakistan; dr.sammer.yousuf@gmail.com or dr.sammer.yousuf@iccs.edu

<sup>3</sup> Department of Chemistry, University of Jyväskylä, P.O. Box 35, FI-40014 Jyväskylä, Finland; matti.o.haukka@jyu.fi

<sup>4</sup> Department of Chemistry, Faculty of Science, Alexandria University, P.O. Box 426, Ibrahimia, Alexandria 21321, Egypt; ayman.elfaham@alexu.edu.eg (A.E.-F.); saeed.soliman@alexu.edu.eg (S.M.S.)

<sup>5</sup> Department of Chemistry, College of Sciences, University of Sharjah, Sharjah P.O. Box 27272, United Arab Emirates; mohamed\_nafie@science.suez.edu.eg

<sup>6</sup> Chemistry Department, Faculty of Science, Suez Canal University, Ismailia 41522, Egypt

\* Correspondence: ambarakat@ksu.edu.sa

**Abstract:** The synthesis and X-ray structure analysis of the new  $[PdLCl_2] \cdot 0.5 CH_2Cl_2$  complex where **L** is hydrazono-*s*-triazine di-morpholine derivative, were presented. In the neutral inner sphere of this complex, the organic ligand **L** is acting as a *NN*-bidentate chelate via the pyridine and hydrazone N-atoms. The coordination configuration of the Pd(II) is completed by two chloride ions at *cis*-positions. The tetra-coordinated Pd(II) showed a distorted square planar geometry. The outer sphere comprised half methylene chloride molecule per  $[PdLCl_2]$  as crystal solvent. The crystal stability is dominated by a number of weak C-H...N, C-H...Cl, and C-H...O non-covalent interactions. Based on Hirshfeld analysis, the H...H, N...H, H...Cl, O...H, Pd...C, and Cl...C intermolecular interactions contributed by 45.2, 9.3, 21.5, 5.8, 2.3, and 3.4%, respectively. DFT studies revealed closed shell characters for the Pd-N and Pd-Cl coordinate bonds. The net charge of Pd is also predicted to be 0.311 e and the amount of electron density transferred from the ligand groups is 1.689 e. The Pd(II) complex exhibited potent cytotoxic activity against MCF-7, HepG2, and A549 cells with  $IC_{50}$  values of 1.18, 4.74, and 5.22  $\mu g/mL$ , compared to cisplatin with  $IC_{50}$  values of 4.1, 9.7, and 12.3  $\mu g/mL$ , respectively. Additionally, it exhibited poor cytotoxicity against WISH cells with much higher  $IC_{50}$  values ( $IC_{50} = 37.2 \mu g/mL$ ). Investigating apoptosis-induction, the Pd(II) complex induced apoptotic cell death by an 11-fold change in MCF-7 cells arresting the cell phase at the G0–G1 phase. Accordingly, Pd(II) complex can be developed as a promising anti-breast cancer agent.

**Keywords:** Pd(II); Hirshfeld; *s*-triazine; hydrazone; anticancer; apoptosis-induction in MCF-7



**Citation:** Alayyaf, A.A.; Barakat, A.; Al-Majid, A.M.; Ali, M.; Yousuf, S.; Haukka, M.; El-Faham, A.; Soliman, S.M.; Nafie, M.S. Cytotoxicity and Apoptosis-Induction in MCF-7 Cells for New Pd(II) Complex Based on *s*-Triazine Ligand: Synthesis, Single Crystal X-ray Diffraction Analysis and Structural Investigations. *Crystals* **2023**, *13*, 1472. <https://doi.org/10.3390/cryst13101472>

Academic Editor: Sergey V. Krivovichev

Received: 3 September 2023

Revised: 4 October 2023

Accepted: 6 October 2023

Published: 10 October 2023



**Copyright:** © 2023 by the authors. Licensee MDPI, Basel, Switzerland. This article is an open access article distributed under the terms and conditions of the Creative Commons Attribution (CC BY) license (<https://creativecommons.org/licenses/by/4.0/>).

## 1. Introduction

Metal complexes based on ligands comprising the *s*-triazine scaffold have sparked the attention of many scientists because this class of metal chelates exhibits many interesting applications [1]. As metal-based catalysts, Pd(II) complexes have been employed in many catalytic transformations such as the polymerization of olefin [2], *ortho*-alkynyl aryl ketones [3], cross-coupling reactions [4] (e.g., Suzuki-Miyaura and Heck reactions), asymmetric allylic alkylation [5], and chain transfer reactions [6] as clean, efficient, and selective methods in synthetic chemistry [1].

On the other hand, many chelating ligands based on the *s*-triazine nucleus were constructed and explored in the field of organometallic chemistry for different purposes, such as catalytic transformation, pharmaceutical [7–14] and photophysical applications [15], corrosion inhibitors [16], optical switches [17,18], dye applications [19], plastics [20], wastewater treatments [21], electrical [22] and energetic explosives as nitrogen-rich molecules [23], in crystal engineering [24,25] because of the symmetric structure of *s*-triazine core, and as MOF for flame retardant apparatus, smoke suppression, and toxin attenuation of epoxy resin (EP) [26]. In the field of pharmacological applications, the metal complexes based on *s*-triazine gained great biological interest for their anti-cancer [8,9,27,28], antimicrobial [29], anti-viral, anti-inflammatory [30], anti-HIV [31,32], and anti-diabetic insulin mimetic [33] properties, among others [34,35].

Many metal complexes comprising *s*-triazine ligands with different metal ions, such as Zn, Mn, Co, Cu, Pt, Pd, and others, were constructed [1]. In particular, Pd(II)-*s*-triazine complexes were synthesized, and assessed for their anti-cancer reactivity. These Pd(II) complexes exhibited high efficacy against MDA-MB-231 and MCF-7 cancer cell lines [36–38]. Another representative example based on *s*-triazine derivatives coordinated with Pd(II) and Pt(IV) was explored for anti-cancer and anti-microbial applications [39]. Ismail et al. designed and synthesized mixed ligand Pd, Pt, and Ag complexes involving *s*-triazine derivatives with other ligands and then explored their DNA binding intercalation [40].

In this regard, the design of new *s*-triazine-based ligands for the construction of new coordination compounds is still an attractive task for researchers. Based on the findings mentioned above and in continuation of our interest in this field [41,42], our aim is to synthesize a new Pd(II) complex based on an *s*-triazine hydrazono-type ligand. Its X-ray structure, combined with Hirshfeld surface analysis, AIM, and NBO studies, was used to analyze the molecular structures of the new Pd(II) complex. Cytotoxicity against three cancer MCF-7, HepG2, and A549 cell lines and apoptosis-induction in MCF-7 cells were also investigated.

## 2. Materials and Methods

General Notes: “The starting materials required for the synthesis of the Pd(II) complex are commercial available unless is stated such as the synthesis of L. NMR data was recorded in CDCl<sub>3</sub> at Joel (400 MHz). IR spectrum recorded by using KBr disc technique using a Nicolet 6700 FT-IR spectrophotometer. The X-ray diffraction data were collected on Bruker D8 Venture X-ray diffractometer (Bruker, Karlsruhe, Germany), which was equipped with a CMOS PHOTON II detector.”

### 2.1. Synthesis of L

The synthesis of the desired ligand was prepared according to our previously reported method and all spectral data are matched with the reported literature [43,44]. In summary, the *bis*-morpholino-*s*-triazine hydrazine reacted with 2-acetyl pyridine in refluxing ethanol with a catalytic amount of the acetic acid for 24 h to afford the desired ligand as white ppt.

### 2.2. Synthesis of the Pd(II) Complex

A mixture of L (~0.192 g, 0.5 mmol) was mixed with PdCl<sub>2</sub> (0.90 g, 0.5 mmol) in 20 mL acetone and stirred at 50° for three days. The solution was filtered off in order to remove undissolved starting materials, and the filtrate was kept at RT for one week for slow evaporation. An orange crystalline compound which is suitable for single-crystal X-ray diffraction analysis was obtained.

Pd(II) complex (C<sub>18</sub>H<sub>24</sub>Cl<sub>2</sub>N<sub>8</sub>O<sub>2</sub>Pd): <sup>1</sup>HNMR (CDCl<sub>3</sub>, 400 MHz) δ 2.43 (s, 3H, CH<sub>3</sub>), 3.75 (t, *J* = 4.8 Hz, 8H, Morpholine), 3.84 (q, *J* = 8.2, 4.6 Hz, 8H, Morpholine), 7.23 (d, *J* = 7.5 Hz, 1H, Ph), 7.70 (t, *J* = 8.0 Hz, 1H, Ph), 8.10 (s, 1H, NH), 8.23 (d, *J* = 8.0 Hz, 1H, Ph), 8.56 (d, *J* = 4.6 Hz, 1H, Ph); <sup>13</sup>CNMR (CDCl<sub>3</sub>, 100 MHz) δ 43.8, 67.0, 119.9, 123.7, 136.3, 139.0, 147.5, 164.6, 165.4; IR (KBr, CM<sup>-1</sup>, ν): 3443 (NH), 2960, 2893, 2854 (C-H, Sp<sup>3</sup>), 1600, 1580, 1520, 1490 (C=C and C=N); and *m/z*: 561.01 [H<sup>+</sup>].

### 2.3. Crystal Structure Determination

The crystallographic measurement for the studied complex was performed using a similar protocol in the literature [45–49].

### 2.4. Hirshfeld Surface Analysis

The topology analyses were performed using the Crystal Explorer 17.5 program [50].

### 2.5. DFT Calculations

All details regarding DFT calculations are described in Supplementary Data [51–57].

### 2.6. Cytotoxicity Using MTT Assay

Breast (MCF-7), liver (HepG2), and lung (A549) cancer cells were obtained and cultured in a complete medium of RPMI-1640 medium L-Glutamine (Lonza, Verviers, Belgium, cat#12-604F). On the second day, cells were exposed to the compounds in concentrations of (0.01, 0.1, 1, 10, and 100  $\mu\text{g}/\text{mL}$ ). Cell viability was assessed using MTT solution (Promega, Madison, WI, USA) after 48 h [58,59].

### 2.7. Annexin V/PI Staining and Cell Cycle Analysis

First,  $3 \times 10^5$  MCF-7 cells were added to 6-well culture plates for the night. Following that, cells were treated with the Pd (II) complex at its  $\text{IC}_{50}$  level for 48 h. Following that, PBS was rinsed with ice-cold water before cells and media supernatants were gathered. The cells were then treated with “Annexin V-FITC solution (1:100) and propidium iodide (PI)” at a concentration of 10  $\mu\text{g}/\text{mL}$  for 30 min in the dark after being suspended in 100 L of annexin binding buffer solution. Then, labeled cells were collected using the Cytoflex FACS system (Beckman Coulter Life Sciences, Loveland, CO, USA). The data were assessed using the cytExpert program [60,61].

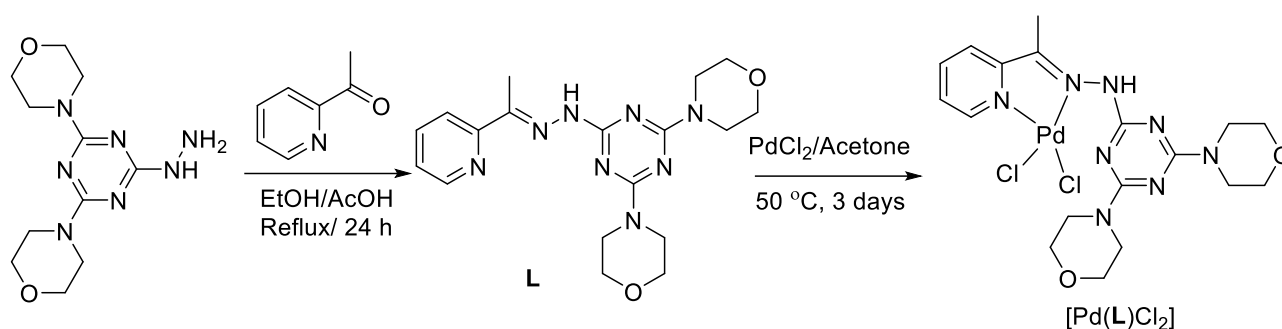
### 2.8. Molecular Docking

Following standard protocols, Pd(II)-Complex was docked to the EGFR (PDB = 1M17) protein structure using AutoDock Vina that obtain the best possible energy optimization between protein and ligand structures. The binding activities were explained in terms of the binding energy and the interactions between the ligand and the receptor. Then, Chimera software was utilized to visualize the binding modes [62].

## 3. Results and Discussion

### 3.1. Synthesis

The hydrazone derivative based on *s*-triazine motif **L** was designed and synthesized for use as a ligand in coordination chemistry not only for Ni (II), Mn (II), and Cu(II) but also to explore with Pd(II). The requisite hydrazono derivative **L** was synthesized according to the El-Faham method in which the 2-acetyl pyridine reacted with the hydrazine derivative under reflux conditions for one day in the presence of a catalytic amount of AcOH. The synthesized hydrazone ligand **L** was then mixed with the  $\text{PdCl}_2$  in a 1:1 molar ratio and stirred for 3 days in acetone under heating at 50  $^\circ\text{C}$  (Scheme 1). The reaction mixture was filtered off then, after slow evaporation, the solid crystalline product of the target complex was collected by filtration. The single crystals of the Pd(II) complex were found suitable for single-crystal X-ray diffraction analysis.



**Scheme 1.** Synthesis of the Pd(II)-complex.

### 3.2. Crystal Structure Description

The structure of the studied Pd(II) complex is shown in Figure 1. The formula of the neutral palladium complex comprised one [Pd(L)Cl<sub>2</sub>] unit and half methylene chloride molecule as a crystallized solvent. Hence, the structure of this complex is [Pd(L)Cl<sub>2</sub>]\*0.5CH<sub>2</sub>Cl<sub>2</sub> in which the Pd(II) is tetra-coordinated with one organic ligand unit (L) as a bidentate *NN*-chelate via the pyridine and the hydrazone nitrogen atoms. The respective Pd1-N1 (2.031(2) Å) and Pd1-N2 (2.012(2) Å) distances are marginally different (Table 1). The bite angle of the bidentate chelate is 79.60(7)°. The coordination environment of the Pd(II) complex is completed by two chloride ions coordinated to the Pd(II) in *cis*-positions. The Pd1-Cl1 and Pd1-Cl2 distances are found to be 2.2843(6) and 2.2911(6) Å, respectively, while the Cl1-Pd1Cl2 angle is 91.66(2)° which is close to the ideal value of a square planar geometrical structure. The rest of the *cis*-bond angles are in the range of 93.82(5)–94.87(6)° while the corresponding values for the *trans*-bond angles are 173.77(5)° and 173.37(6)° for N2-Pd1-Cl1 and N1-Pd1-Cl2, respectively (Table 2). Hence, the coordination geometry around Pd(II) is typically square planar with some distortion.

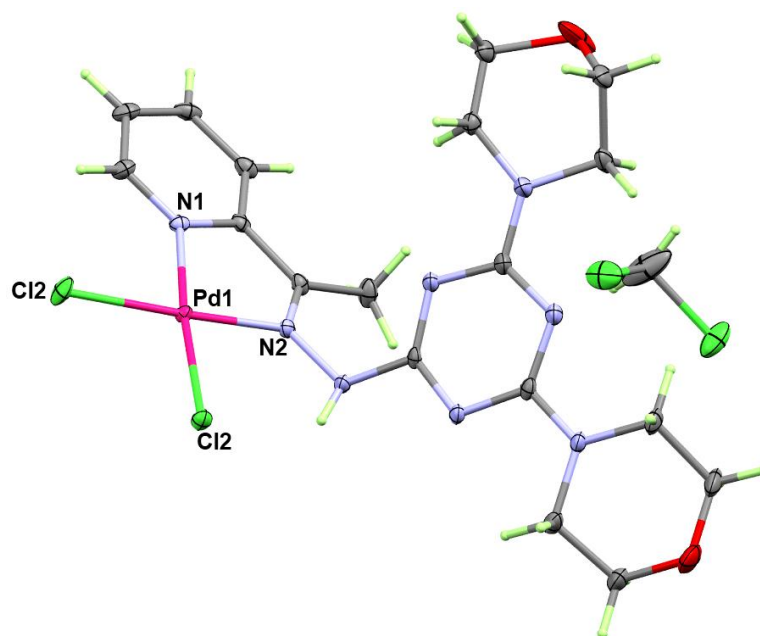


**Figure 1.** Structure with atom numbering of the studied Pd(II) complex. One of the morpholine moieties showed disorder, as shown in Figure S1 (Supplementary Data).

**Table 1.** Crystal data and structure refinement for the studied Pd(II) complex.

CCDC	2245968
Empirical formula	C <sub>18.5</sub> H <sub>25</sub> N <sub>8</sub> O <sub>2</sub> Cl <sub>3</sub> Pd
Formula weight	604.21
Temperature/K	103(2)
Crystal system	monoclinic
Space group	C2/c
a/Å	34.3742(18)
b/Å	10.2427(6)
c/Å	14.0115(8)
β/°	109.518(2)
Volume/Å <sup>3</sup>	4649.8(5)
Z	8
ρ <sub>calc</sub> /cm <sup>3</sup>	1.726
μ/mm <sup>−1</sup>	9.909
F(000)	2440
Crystal size/mm <sup>3</sup>	0.3 × 0.07 × 0.035
Radiation	CuKα (λ = 1.54178)
2θ range for data collection/°	9.054 to 136.48
Index ranges	−41 ≤ h ≤ 41, −12 ≤ k ≤ 11, −16 ≤ l ≤ 16
Reflections collected	65400
Independent reflections	4242 (R <sub>int</sub> = 0.0402, R <sub>sigma</sub> = 0.0148)
Data/restraints/parameters	4242/0/331
Goodness-of-fit on F <sup>2</sup>	0.995
Final R indexes [I ≥ 2σ (I)]	R <sub>1</sub> = 0.0256, wR <sub>2</sub> = 0.0669
Final R indexes [all data]	R <sub>1</sub> = 0.0263, wR <sub>2</sub> = 0.0675
Largest diff. peak/hole/e Å <sup>−3</sup>	0.50/−0.98

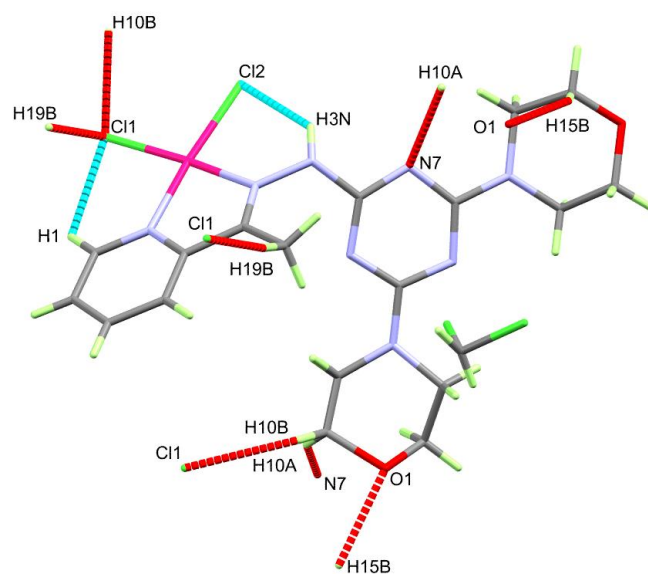
**Table 2.** Bond lengths (Å) and angles (°) for the studied Pd(II) complex.

Bond	Length/Å	Bond	Length/Å
<b>Bond distances</b>			
Pd1-N1	2.031(2)	Pd1-Cl1	2.2843(6)
Pd1-N2	2.012(2)	Pd1-Cl2	2.2911(6)
<b>Bond angles</b>			
Cl1-Pd1-Cl2	91.66(2)	N2-Pd1-Cl1	173.77(5)
N1-Pd1-Cl1	94.87(6)	N2-Pd1-Cl2	93.82(5)
N1-Pd1-Cl2	173.37(6)	N2-Pd1-N1	79.60(7)

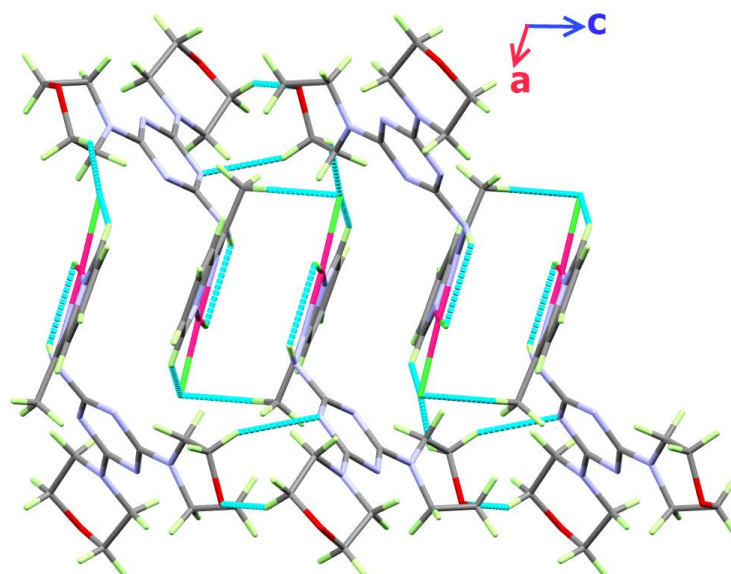
The molecular unit [Pd(L)Cl<sub>2</sub>] comprised two intra-molecular interactions between the coordinated chloride anions and the neighboring N-H and C-H bonds. The donor-acceptor distances of the respective N3-H3N...Cl2 and C1-H1...Cl1 interactions are 3.161(2), and 3.273(2) Å, respectively (Table 3). These intra-molecular contacts are presented in Figure 2 as a turquoise dotted line.

**Table 3.** Hydrogen bonds for the studied Pd(II) complex (Å and °).

D-H...A	d(D-H)	d(H...A)	d(D...A)	<(DHA)	Symm. Code
N3-H3N...Cl2	0.84(3)	2.55(4)	3.161(2)	131(3)	
C1-H1...Cl1	0.95	2.69	3.273(2)	120	
C10A-H10A...N7	0.99	2.61	3.491(6)	148	$x, 1 - y, 1/2 + z$
C10A-H10B...Cl1	0.99	2.71	3.565(5)	144	$1/2 - x, 1/2 + y, 1/2 - z$
C15-H15B...O1	0.99	2.41	3.300(4)	150	$x, 1 - y, -1/2 + z$
C19-H19B...Cl1	0.98	2.74	3.717(3)	172	$1/2 - x, 3/2 - y, -z$

**Figure 2.** The possible intra-molecular (turquoise) and inter-molecular (red) contacts in the studied Pd(II) complex. The details of their geometrical parameters are depicted in Table 3.

Additionally, the packing of the complex units is controlled by a number of weak C-H...N, C-H...Cl and C-H...O non-covalent interactions. The presentation of these contacts is shown as a red dotted line in Figure 2, while the packing structure for this complex is illustrated in Figure 3.

**Figure 3.** Packing structure for the studied Pd(II) complex along *ac* plane.

### 3.3. Analysis of Molecular Packing

The intermolecular interactions in the crystalline solid structure have great impacts on the crystal stability. In this regard, the different intermolecular contacts affecting the crystal stability were analyzed using Hirshfeld surface analysis (Figure 4). In the  $d_{\text{norm}}$  map, the short significant contacts appeared as red spots while the less important intermolecular interactions appeared as blue or white areas. A summary of the intermolecular contacts and their percentage contributions are depicted in Figure 5.

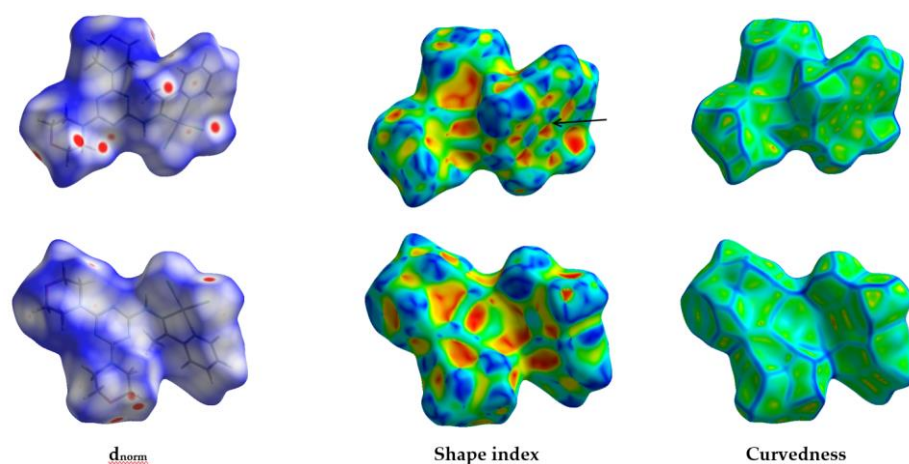


Figure 4. Hirshfeld surfaces of the Pd(II) complex.

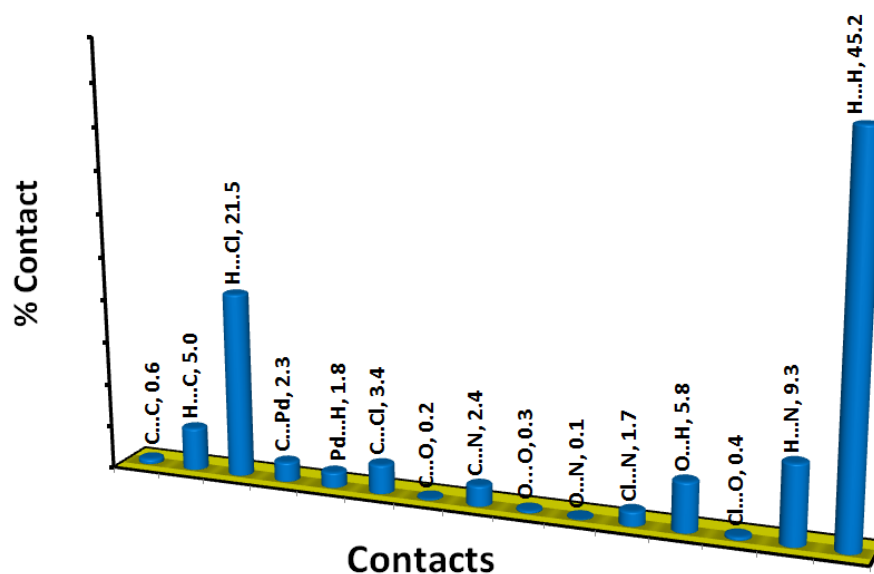


Figure 5. Summary of the intermolecular interactions and their percentages.

In the  $d_{\text{norm}}$  Hirshfeld surface of the studied Pd(II) complex, there are many significant contacts such as H...H, N...H, H...Cl, O...H, Pd...C, and Cl...C interactions. All these contacts appeared as red regions indicating shorter distances than the van der Waals radii sum of the interacting atoms (Figure 6). These contacts contributed 45.2, 9.3, 21.5, 5.8, 2.3, and 3.4% of the whole fingerprint area (Figure 7). In addition, the majority of these interactions appeared as sharp spikes in the decomposed fingerprint plots, which are considered to be another feature of the short and significant contacts.



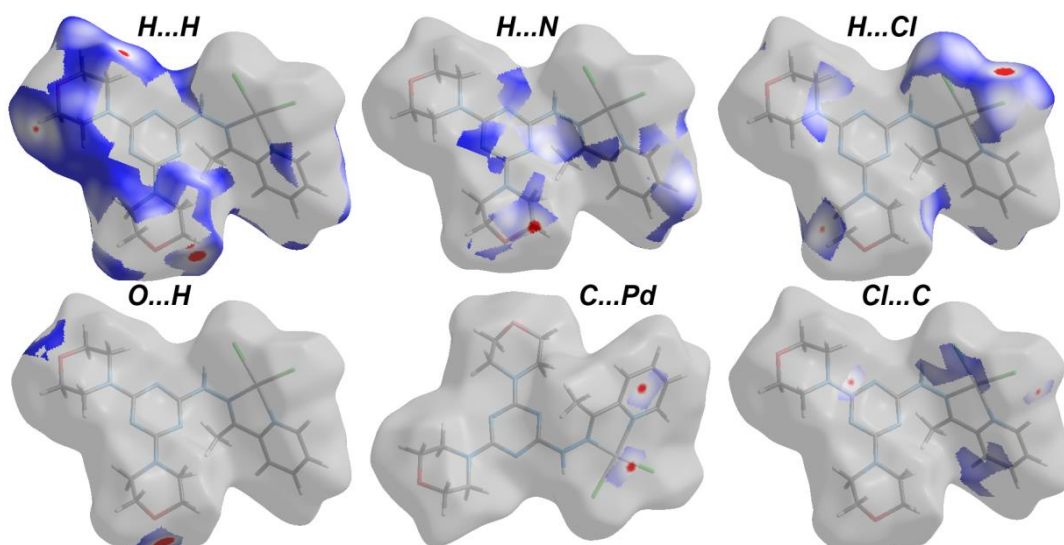


Figure 6. Full and decomposed  $d_{\text{norm}}$  maps for the important interactions in the Pd(II) complex.

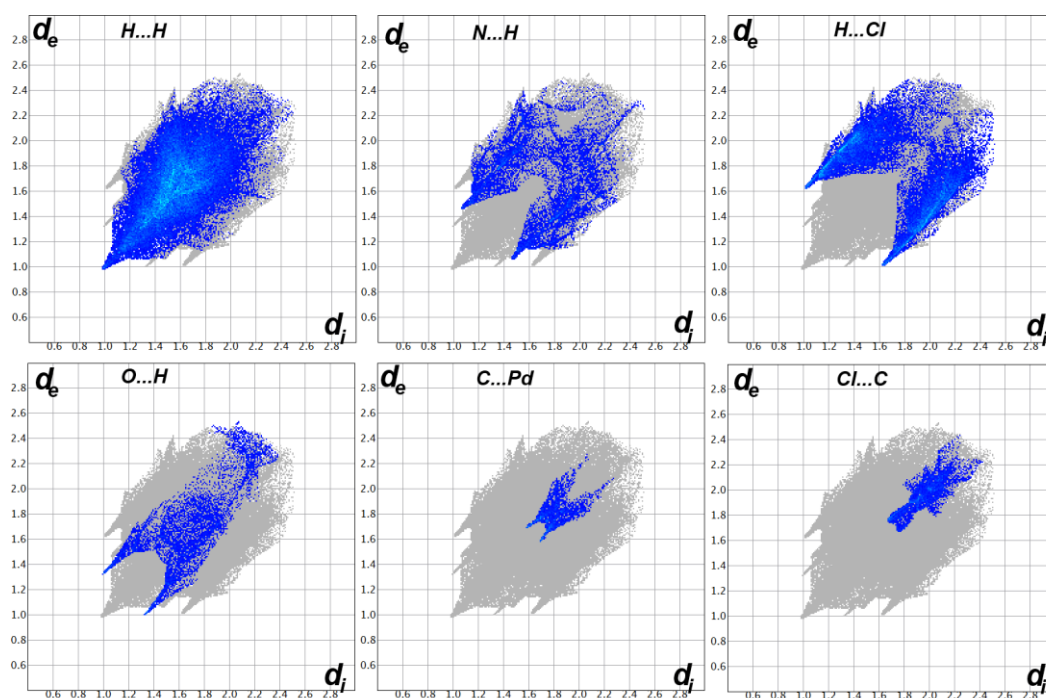


Figure 7. Full and decomposed fingerprint plots for the important interactions in the Pd(II) complex.

Analysis of the interaction distances for these important contacts is listed in Table 4. There are two short H...H interactions which are H3...H13 and H20...H20. The corresponding interaction distances are 1.972 and 2.152 Å, respectively. As can be seen from Table 4, three Cl...H interactions occurred between the protons of the aliphatic C-H groups from one side and one of the coordinated chlorides (Cl1) and the chlorine atom of the crystallized solvent molecule from the other side. These contacts are Cl1...H4, Cl1...H22, and Cl3...H6, while the corresponding interaction distances are 2.637, 2.642, and 2.823 Å, respectively. Other short contacts such as Pd1...C8 (3.278 Å), C12...Cl3 (3.439 Å), C19...O2 (3.002 Å), O1...H16 (2.327 Å), and H3...N7 (2.533 Å) also have shorter contact distances than the vdWs radii sum of the two atoms sharing this contact (Table 4).

**Table 4.** Summary of the intermolecular interactions based on Hirshfeld analysis.

Contact	Distance	Contact	Distance
C11...H4	2.637	C19...O2	3.002
C11...H22	2.642	H3...H13	1.972
Cl3...H6	2.823	H20...H20	2.152
Pd1...C8	3.278	O1...H16	2.327
C12...Cl3	3.439	H3...N7	2.533

Interestingly, the Hirshfeld analysis revealed the presence of some weak  $\pi$ - $\pi$  stacking interactions. As clearly seen from the shape index map presented in Figure 4, there are blue/red triangles indicated by black arrows which are the main characteristic of  $\pi$ - $\pi$  stacking interactions. The shortest ring-ring contact is 3.394 Å (C10...N1), which is slightly longer than the VDWs radii sum of C and N atoms (3.25 Å). The net percentage of the C...N contacts is 2.4%.

### 3.4. The Atoms in Molecules (AIM) Analysis

Understanding the nature of bonding is one of the interesting topics in chemistry. The theory of AIM is the most suited for this task. In this regard, analysis of the coordination interactions was performed with the aid of the topological parameters presented in Table 5 [63–69]. Analysis of the electron density  $\rho(r)$  and its laplacian  $\nabla^2\rho(r)$  indicated mainly closed-shell Pd-N and Pd-Cl interactions. The electron density  $\rho(r)$  values are small and less than 0.1 a.u., and the  $\nabla^2\rho(r)$  values are also small. Additionally, the total energy density, which is the sum of the kinetic energy density  $G(r)$  and potential energy density  $V(r)$ , has small negative values (−0.03 to −0.08 a.u.) which confirm that the Pd-N and Pd-Cl interactions have a predominantly closed-shell character with little covalency. On the other hand, the values of  $\rho(r)$  are higher for the shorter Pd1-N2 and Pd1-Cl1 bonds compared to the Pd1-N1 and Pd1-Cl2 bonds, respectively. It is clear that there is an inverse relation between the electron  $\rho(r)$  and bond strength.

**Table 5.** AIM topology parameters (a.u.) at Pd-N and Pd-O bond critical points (BCPs).

Bond	P (r)	G (r)	V (r)	H (r)	$\nabla^2\rho$ (r)
Pd1-N1	0.0736	0.1789	−0.1868	−0.0079	0.6843
Pd1-N2	0.0747	0.1918	−0.1995	−0.0076	0.7367
Pd1-Cl1	0.0892	0.0793	−0.1062	−0.0269	0.2095
Pd1-Cl2	0.0879	0.0781	−0.1043	−0.0261	0.2080

### 3.5. Natural Population Analysis

Analysis of the net charges of the ligand groups and the central metal ion sheds light on the Lewis acid-base interactions among them. Natural charge analysis [70] is one of the most suitable methods for charge calculations. The charge of the Pd(II) ion is changed to +0.311 e instead of +2.000. The significant decrease in the charge of the Pd(II) is attributed to the charge transfer interactions from the ligand groups to the central Pd(II) ion. The amount of electron density transferred from the organic ligand is 0.483 e while the two chloride ions transferred almost the same amount of electron density (0.6041 and 0.6020 e). Hence, the net number of electrons transferred from the ligand groups is 1.689 e.

### 3.6. Cytotoxic Activity

The tested compounds were screened for their cytotoxicity against breast MCF-7, HepG2, and A549 cell lines using MTT assay. The cytotoxicity results of the Pd(II) complex exhibited potent cytotoxic activity against MCF-7, HepG2, and A549 cells with  $IC_{50}$  values of 1.18, 4.74, and 5.22  $\mu\text{g/mL}$ , compared to erlotinib as a standard anti-EGFR drug with  $IC_{50}$  values of 1.32, 6.5, 5.6  $\mu\text{g/mL}$ , respectively (Table 6). Additionally, Pd(II) complex exhibited potent cytotoxicity against MCF-7, HepG2, and A549 cells compared to cisplatin

as a standard drug, which exhibited  $IC_{50}$  values of 4.1, 9.7, and 12.3  $\mu\text{g}/\text{mL}$ , and compared to doxorubicin with  $IC_{50}$  values of 3.4, 8.3 and 7.9  $\mu\text{g}/\text{mL}$ , respectively. The Pd(II) complex treatment induced potent cell growth inhibition at the highest concentration (100  $\mu\text{g}/\text{mL}$ ) as shown in Figure 8. Additionally, when Pd(II) complex was investigated for its cytotoxicity against WISH cells, it exhibited poor cytotoxicity with much higher  $IC_{50}$  values ( $IC_{50} = 37.2 \mu\text{g}/\text{mL}$ ) than in cancer cells. Accordingly, Pd(II) complex was more cytotoxic against cancer cells compared to doxorubicin and cisplatin with poor cytotoxicity against normal cells.

**Table 6.** The  $IC_{50}$  values for Pd(II) complex against MCF-7, HepG2, and A549 cancer cells using MTT assay.

	$IC_{50} \pm SD [\mu\text{g}/\text{mL}]^*$			
	MCF-7	HepG2	A549	Normal WISH Cells
<b>Pd(II)-Complex</b>	$1.18 \pm 0.1$	$4.74 \pm 0.25$	$5.22 \pm 0.36$	$37.2 \pm 1.8$
<b>Erlotinib</b>	$1.32 \pm 0.04$	$6.53 \pm 0.2$	$5.65 \pm 0.3$	$43.8 \pm 2.0$
<b>Cisplatin</b>	$4.1 \pm 0.1$	$9.76 \pm 0.2$	$12.34 \pm 0.3$	$32.7 \pm 1.5$
<b>Doxorubicin</b>	$3.4 \pm 0.05$	$8.3 \pm 0.1$	$7.9 \pm 0.1$	$\geq 50$

\*  $IC_{50}$  values were calculated by non-linear regression curve fit using GraphPad prism. Erlotinib as standard EGFR inhibitor.

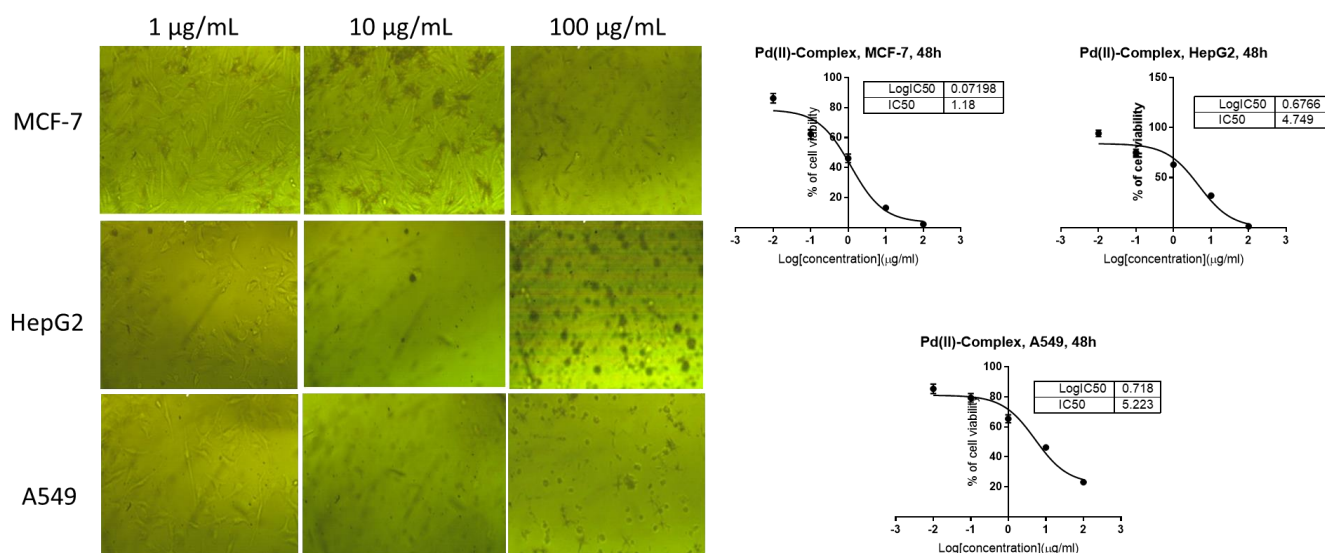


**Figure 8.** (Left panel) Morphological assessment of MCF-7, HepG2, and A549 cell lines upon treatment of Pd(II) complex for 48h. (Right panel) Percentage of cell viability of MCF-7, HepG2, and A549 cells vs.  $\log [\text{con. } \mu\text{g}/\text{mL}]$ ,  $R^2 \approx 1$  using the GraphPad prism 7 software.

The results of our study agree with Fernández-Delgado et al. [71], who synthesized new Pd(II) complexes with thiazine or thiazoline derivative and investigated their cytotoxicities against tumor cells through apoptosis. Additionally, our results agree with Sun et al. [72], who synthesized Pd(II) and Pt(II) complexes containing pyridine carboxylic acid and investigated them as cytotoxic agents against cancer cells through DNA interactions.

### 3.7. Apoptosis-Induction Activity (Annexin V/PI Staining and Cell Cycle Analysis)

Annexin V/PI staining was used to examine the cytotoxic activity of Pd(II) complex in MCF-7 cells and determine the mechanism by which apoptosis was induced. Figure 9 shows that compared to control cells (3.9%), Pd(II) complex treatment increased total apoptotic cell death in the MCF-7 cells by 42.9%. So, it induced apoptosis by an 11-fold

change. Furthermore, it resulted in a 5.3% increase in necrotic cell death compared to a 0.346% decrease in cell death in the untreated control group.

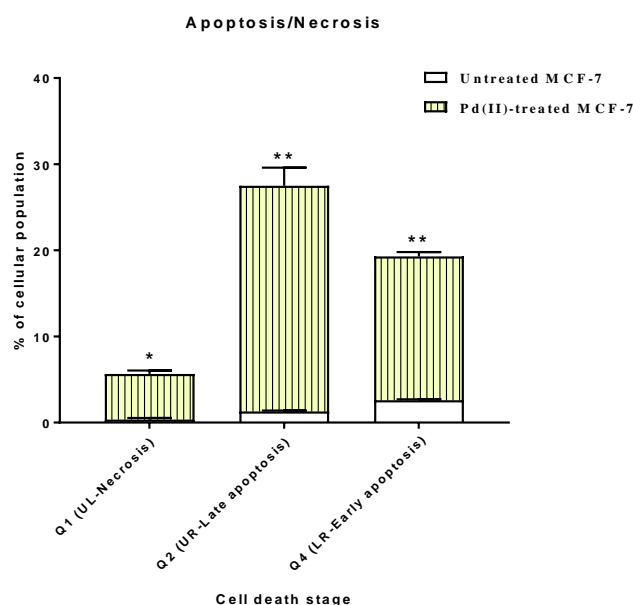


**Figure 9.** Bar presentation of apoptosis/necrosis activity using flow cytometry using Annexin V/PI staining in the untreated and treated MCF-7 cancer cells ( $IC_{50} = 1.18 \mu\text{g/mL}$ , 48 h). Values are expressed as Mean  $\pm$  SD of two independent trials. “Statistical significance \* ( $p \leq 0.05$ ) and \*\* ( $p \leq 0.001$ ) using unpaired *t*-test in GraphPad software”.

Cell cycle analysis was performed on MCF-7 cells, showing the percentage of cells in each phase of the cell cycle for both control and treated samples, to determine which stage of the cell cycle arresting effect was most prominent. As seen in Figure 10, the Pd(II) complex significantly elevated the cell population at the G0–G1 phase by 49.18%, compared to 31.8% (control), so it arrested the cell cycle at the G0–G1 phase. Upon treatment, the cell population in the S-phase non-significantly increased, while the cell population in the G2/M phase decreased. Accordingly, the Pd(II) complex arrested the cell proliferation of MCF-7 cells in the G0–G1 phase.

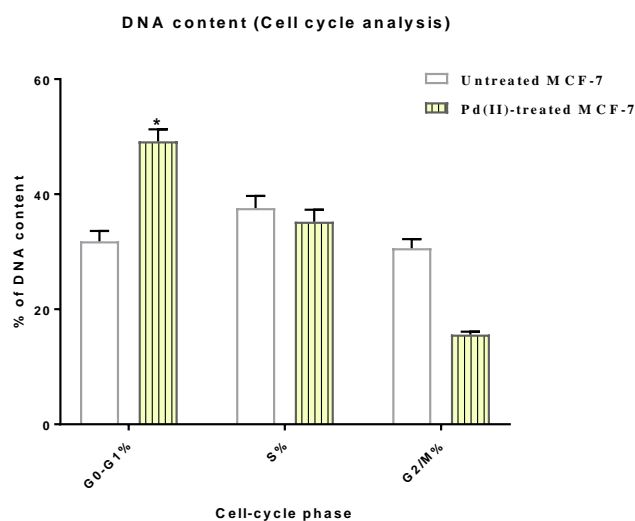


**Figure 10.** Bar chart for the DNA-aided cell cycle analysis with the cell population at each cell phase (G0–G1, S, G2/M phases) in untreated and Pd(II) complex-treated MCF-7 cells ( $IC_{50} = 1.18 \mu\text{g/mL}$ , 48 h). \* ( $p \leq 0.05$ ) significantly different between untreated and treated groups using unpaired *t*-test in Graphpad prism.

### 3.8. Molecular Docking

Epidermal growth factor receptor (EGFR) is a transmembrane receptor protein that is an extracellular protein in humans. The receptor becomes available to bind intracellular effector proteins after autophosphorylation of intracellular tyrosine residues. This interaction promoted cell growth, cell invasion, angiogenesis, metastasis, resistance to apoptosis, and DNA repair. Breast cancer is just one of several types of malignancy that can result from alterations to the EGFR gene, such as mutations, rearrangements, overexpression, or amplification. So, EGFR inhibition is a promising therapeutic target as EGFR kinase receptors are the major investigated targets in many cancer types [73,74].

The molecular docking study highlighted virtually the mechanism of binding of Pd(II)-Complex towards the EGFR that highlighted the molecular target. As seen in Figure 11, Pd(II)-Complex exhibited the same binding mode of the co-crystallized ligand, and it had binding energy of  $-21.72$  Kcal/mol, and formed two H-bonds with Meth 769 and Lys 721 as the key amino acids for EGFR enzyme activity.

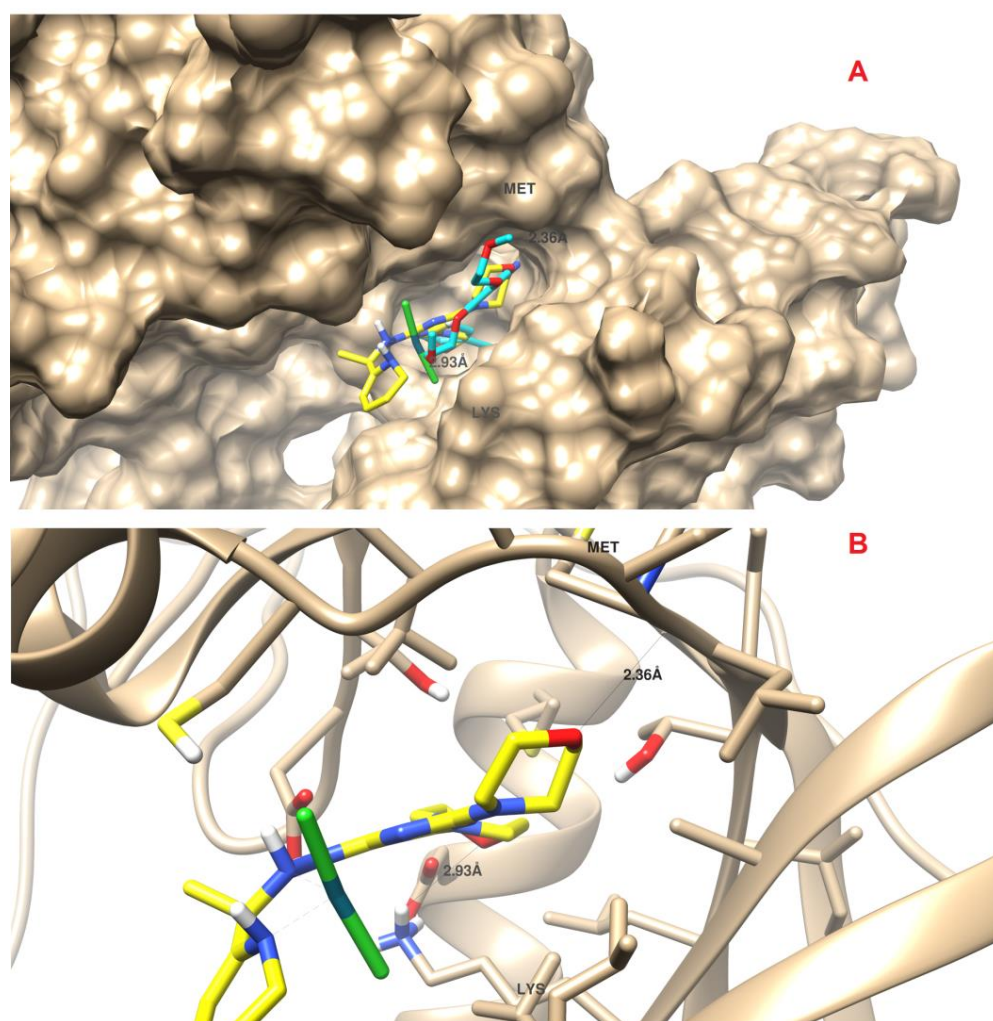


**Figure 11.** Ligand–receptor binding dispositions of docked Pd(II)-Complex inside the EGFR protein. (A) Surface-view of both co-crystallized ligand (Cyan-colored) and Pd(II)-Complex (Yellow-colored) (B) Interactive view with the key amino acids Met 67 of EGFR activity.

### 4. Conclusions

The Pd(II) complex of the hydrazono-*s*-triazine di-morpholine derivative was synthesized and its X-ray structure was reported for the first time. The X-ray structure revealed a distorted square planar coordination geometry with one organic ligand **L** as a bidentate chelate and two chloride ions at *cis*-position. In addition to the [PdLCl<sub>2</sub>], the structure of

the complex showed half methylene chloride molecule as a crystal solvent in the inner sphere. Hence, the structure of the Pd(II) complex is  $[\text{PdLCl}_2] \cdot 0.5\text{CH}_2\text{Cl}_2$ . Supramolecular structure analysis for the crystal packing was presented based on Hirshfeld analysis. It is found that the H...H, N...H, H...Cl, O...H, Pd...C, and Cl...C non-covalent interactions are the most important. Their percentages are 45.2, 9.3, 21.5, 5.8, 2.3, and 3.4%, respectively. AIM analysis indicated closed-shell characters for the Pd-N and Pd-Cl coordinate bonds, while NBO analysis predicted the amount of electron density transferred from the ligand group to Pd(II) to be 1.689 e. Pd(II) complex exhibited potent cytotoxic activity against MCF-7 with an  $\text{IC}_{50}$  value of 1.18  $\mu\text{g}/\text{mL}$ , compared to doxorubicin, erlotinib, and cisplatin as standard drugs. Additionally, it exhibited poor cytotoxicity against WISH cells with much higher  $\text{IC}_{50}$  values ( $\text{IC}_{50} = 37.2 \mu\text{g}/\text{mL}$ ). Investigating apoptosis-induction, it induced apoptotic cell death by an 11-fold change in MCF-7 cells arresting the cell phase at the G0–G1 phase. Accordingly, Pd(II) complex can be considered a promising anti-breast cancer agent through apoptosis-induction.

**Supplementary Materials:** The following supporting information can be downloaded at: <https://www.mdpi.com/article/10.3390/cryst13101472/s1>, Figure S1: Structure of the studied Pd(II) complex showing the morpholine disorder. X-ray Structure determination; DFT calculations; Cytotoxicity using MTT assay; Investigation of apoptosis.

**Author Contributions:** Conceptualization, A.B. and A.E.-F.; methodology, A.A.A., A.B., and M.A.; software, M.H., S.M.S., S.Y. and M.S.N.; validation, A.M.A.-M., A.E.-F. and S.M.S.; formal analysis, A.A.A., A.B., M.A., M.H., S.M.S., S.Y. and M.S.N.; investigation, A.B. and M.S.N.; resources, A.B. and A.M.A.-M.; data curation, All; writing—original draft preparation, A.B., S.M.S. and M.S.N.; writing—review and editing, All; project administration, M.A.; funding acquisition, A.A.A. All authors have read and agreed to the published version of the manuscript.

**Funding:** The authors would like to extend their sincere appreciation to the Researchers Supporting Project (RSPD2023R527), King Saud University, Riyadh, Saudi Arabia.

**Data Availability Statement:** Not applicable.

**Acknowledgments:** The authors would like to extend their sincere appreciation to the Researchers Supporting Project (RSPD2023R527), King Saud University, Riyadh, Saudi Arabia.

**Conflicts of Interest:** The authors declare no conflict of interest.

## References

1. Barakat, A.; El-Faham, A.; Haukka, M.; Al-Majid, A.M.; Soliman, S.M. S-Triazine pincer ligands: Synthesis of their metal complexes, coordination behavior, and applications. *Appl. Organomet. Chem.* **2021**, *35*, e6317. [CrossRef]
2. Bermesheva, E.V.; Medentseva, E.I.; Khrychikova, A.P.; Wozniak, A.I.; Guseva, M.A.; Nazarov, I.V.; Morontsev, A.A.; Karpov, G.O.; Topchiy, M.A.; Asachenko, A.F.; et al. Air-Stable Single-Component Pd-Catalysts for Vinyl-Addition Polymerization of Functionalized Norbornenes. *ACS Catal.* **2022**, *12*, 15076–15090. [CrossRef]
3. Antony, A.M.; Chamanmalik, M.I.; Kandathil, V.; Sampatkumar, H.G.; Sasidhar, B.S.; Yelamaggad, C.V.; Patil, S.A. Biomacromolecule supported N-heterocyclic carbene-palladium (II) as a novel catalyst for Suzuki–Miyaura and Mizoroki–Heck cross-coupling reactions. *Cellulose* **2023**, *30*, 7551–7573. [CrossRef]
4. Jiang, B.; Zhang, T.S.; Liu, S.; Hao, W.J. Exploiting the reactivities of ortho-alkynyl aryl ketones: Opportunities in designing catalytic annulation reactions. *Org. Chem. Front.* **2023**, *10*, 570–589. [CrossRef]
5. Wang, H.; Xu, Y.; Zhang, F.; Liu, Y.; Feng, X. Bimetallic palladium/cobalt catalysis for enantioselective allylic C–H alkylation via a transient chiral nucleophile strategy. *Angew. Chem.* **2022**, *134*, e202115715. [CrossRef]
6. Lu, Z.; Liao, Y.; Fan, W.; Dai, S. Efficient suppression of the chain transfer reaction in ethylene coordination polymerization with dibenzosuberyl substituents. *Polym. Chem.* **2022**, *13*, 4090–4099. [CrossRef]
7. Shah, D.R.; Modh, R.P.; Chikhahia, K.H. Privileged s-triazines: Structure and pharmacological applications. *Future Med. Chem.* **2014**, *6*, 463–477. [CrossRef]
8. Cascioferro, S.; Parrino, B.; Spanò, V.; Carbone, A.; Montalbano, A.; Barraja, P.; Diana, P.; Cirrincione, G. 1,3,5-Triazines: A promising scaffold for anticancer drugs development. *Eur. J. Med. Chem.* **2017**, *142*, 523–549. [CrossRef]
9. Cascioferro, S.; Parrino, B.; Spanò, V.; Carbone, A.; Montalbano, A.; Barraja, P.; Diana, P.; Cirrincione, G. An overview on the recent developments of 1,2,4-triazine derivatives as anticancer compounds. *Eur. J. Med. Chem.* **2017**, *142*, 328–375. [CrossRef]
10. Yetim, N.K.; Sari, N. Novel dendrimers containing redox mediator: Enzyme immobilization and applications. *J. Mol. Struct.* **2019**, *1191*, 158–164. [CrossRef]

11. Paul, L.E.; Therrien, B.; Furrer, J. The complex-in-a-complex cation [Pt (acac) 2-(p-cym)<sub>6</sub>Ru<sub>6</sub>(tpt)<sub>2</sub>(dhnq)<sub>3</sub>]<sup>6+</sup>: Its stability towards biological ligands. *Inorganica Chim. Acta* **2018**, *469*, 1–10. [[CrossRef](#)]
12. Asman, P.W. Kinetics and mechanistic study of polynuclear platinum (II) polypyridyl complexes; A paradigm shift in search of new anticancer agents. *Inorganica Chim. Acta* **2018**, *469*, 341–352. [[CrossRef](#)]
13. Zhang, W.; Wang, J.; Xu, Y.; Li, W.; Shen, W. Fine tuning phosphorescent properties of platinum complexes via different N-heterocyclic-based C-N-N ligands. *J. Organomet. Chem.* **2017**, *836*, 26–33. [[CrossRef](#)]
14. Zheng, X.H.; Mu, G.; Zhong, Y.F.; Zhang, T.P.; Cao, Q.; Ji, L.N.; Zhao, Y.; Mao, Z.W. Trigeminal star-like platinum complexes induce cancer cell senescence through quadruplex-mediated telomere dysfunction. *Chem. Commun.* **2016**, *52*, 14101–14104. [[CrossRef](#)]
15. He, Z.; Li, M.; Que, W.; Stang, P.J. Self-assembly of metal-ion-responsive supramolecular coordination complexes and their photophysical properties. *Dalton Trans.* **2017**, *46*, 3120–3124. [[CrossRef](#)]
16. El-Faham, A.; Dahlous, K.A.; Al-Othman, Z.A.; Al-Lohedan, H.A.; El-Mahdy, G.A. Sym-trisubstituted 1,3,5-triazine derivatives as promising organic corrosion inhibitors for steel in acidic solution. *Molecules* **2016**, *21*, 436–447. [[CrossRef](#)] [[PubMed](#)]
17. Mahler, J.; Rafler, G. Modified melamine resins for optical applications. *Opt. Mater.* **1999**, *12*, 363–368. [[CrossRef](#)]
18. Nuyken, O.; Scherer, C.; Baidl, A.; Brenner, A.R.; Dahn, U.; Gärtner, R.; Kaiser-Rohrich, S.; Kollefrath, R.; Matusche, P.; Voit, B. Azo-group-containing polymers for use in communications technologies. *Prog. Polym. Sci.* **1997**, *22*, 93–183. [[CrossRef](#)]
19. Naz, A.; Arun, S.; Narvi, S.S.; Alam, M.S.; Singh, A.; Bhartiya, P.; Dutta, P.K. Cu(II)-carboxymethyl chitosan-silane Schiff base complex grafted on nano silica: Structural evolution, antibacterial performance and dye degradation ability. *Int. J. Biol. Macromol.* **2018**, *110*, 215–226. [[CrossRef](#)]
20. Horacek, H.; Pieh, S. The importance of intumescent systems for fire protection of plastic materials. *Polym. Int.* **2000**, *49*, 1106–1114. [[CrossRef](#)]
21. Lu, F.; Astruc, D. Nanomaterials for removal of toxic elements from water. *Coord. Chem. Rev.* **2018**, *356*, 147–164. [[CrossRef](#)]
22. Gonul, I.; Ay, B.; Karaca, S.; Sahin, O.; Serin, S. Novel copper(II) complexes of two tridentate ONN type ligands: Synthesis, characterization, electrical conductivity and luminescence properties. *Inorganica Chim. Acta* **2018**, *477*, 75–83. [[CrossRef](#)]
23. Nedel'ko, V.V.; Shastin, A.V.; Korsunskii, B.L.; Chukanov, N.V.; Larikova, T.S.; Kazakov, A.I. Synthesis and thermal decomposition of ditetrazol-5-ylamine. *Russ. Chem. Bull.* **2005**, *54*, 1710. [[CrossRef](#)]
24. Mooibroek, T.J.; Gamez, P. The s-triazine ring, a remarkable unit to generate supramolecular interactions. *Inorganica Chim. Acta* **2007**, *360*, 381–404. [[CrossRef](#)]
25. Gamez, P.; Reedijk, J. 1,3,5-triazine-based synthons in supramolecular chemistry. *Eur. J. Inorg. Chem.* **2006**, *37*, 29–42. [[CrossRef](#)]
26. Zhang, G.; Wu, W.; Yao, M.; Wu, Z.; Jiao, Y.; Qu, H. Novel triazine-based metal-organic frameworks: Synthesis and multifunctional application of flame retardant, smoke suppression and toxic attenuation on EP. *Mater. Des.* **2023**, *226*, 111664. [[CrossRef](#)]
27. Lolak, N.; Akocak, S.; Bua, S.; Supuran, C.T. Design, synthesis and biological evaluation of novel ureido benzenesulfonamides incorporating 1, 3, 5-triazine moieties as potent carbonic anhydrase IX inhibitors. *Bioorg. Chem.* **2019**, *82*, 117–122. [[CrossRef](#)]
28. Liu, B.; Sun, T.; Zhou, Z.; Du, L. A systematic review on antitumor agents with 1,3,5-triazines. *Med. Chem.* **2015**, *5*, 131–148. [[CrossRef](#)]
29. Soliman, S.M.; Albering, J.H.; Sholkamy, E.N.; El-Faham, A. Mono-and penta-nuclear self-assembled silver (I) complexes of pyrazolyl s-triazine ligand; synthesis, structure and antimicrobial studies. *Appl. Organomet. Chem.* **2020**, *34*, e5603. [[CrossRef](#)]
30. Maliszewski, D.; Drozdowska, D. Recent Advances in the Biological Activity of s-Triazine Core Compounds. *Pharmaceuticals* **2022**, *15*, 221. [[CrossRef](#)] [[PubMed](#)]
31. Patel, R.V.; Kumari, P.; Rajani, D.P.; Pannecouque, C.; De Clercq, E.; Chikhaliya, K.H. Antimicrobial, anti-TB, anticancer and anti-HIV evaluation of new s-triazine-based heterocycles. *Future Med. Chem.* **2012**, *4*, 1053–1065. [[CrossRef](#)]
32. Xiong, Y.-Z.; Chen, F.-E.; Balzarini, J.; De Clercq, E.; Pannecouque, C. Non-nucleoside HIV-1 reverse transcriptase inhibitors. Part 11: Structural modulations of diaryltriazines with potent anti-HIV activity. *Eur. J. Med. Chem.* **2008**, *43*, 1230–1236. [[CrossRef](#)] [[PubMed](#)]
33. Fujimoto, S.; Yasui, H.; Yoshikawa, Y. Development of a novel antidiabetic zinc complex with an organoselenium ligand at the lowest dosage in KK-A(y) mice. *J. Inorg. Biochem.* **2013**, *121*, 10–15. [[CrossRef](#)] [[PubMed](#)]
34. Shawish, I.; Barakat, A.; Aldalbahi, A.; Alshaer, W.; Daoud, F.; Alqudah, D.A.; Al Zoubi, M.; Hatmal, M.M.M.; Nafie, M.S.; Haukka, M.; et al. Acetic acid mediated for one-pot synthesis of novel pyrazolyl s-triazine derivatives for the targeted therapy of triple-negative breast tumor cells (MDA-MB-231) via EGFR/PI3K/AKT/mTOR signaling cascades. *Pharmaceutics* **2022**, *14*, 1558. [[CrossRef](#)]
35. Shawish, I.; Barakat, A.; Aldalbahi, A.; Malebari, A.M.; Nafie, M.S.; Bekhit, A.A.; Albohy, A.; Khan, A.; Ul-Haq, Z.; Haukka, M.; et al. Synthesis and antiproliferative activity of a new series of mono-and bis (dimethylpyrazolyl)-s-triazine derivatives targeting EGFR/PI3K/AKT/mTOR signaling cascades. *ACS Omega* **2022**, *7*, 24858–24870. [[CrossRef](#)]
36. Lasri, J.; Haukka, M.; Al-Rasheed, H.H.; Abutaha, N.; El-Faham, A.; Soliman, S.M. Synthesis, structure and in vitro anticancer activity of Pd (II) complex of pyrazolyl-s-triazine ligand; A new example of metal-mediated hydrolysis of s-triazine pincer ligand. *Crystals* **2021**, *11*, 119. [[CrossRef](#)]
37. Lasri, J.; Al-Rasheed, H.H.; El-Faham, A.; Haukka, M.; Abutaha, N.; Soliman, S.M. Synthesis, structure and in vitro anticancer activity of Pd (II) complexes of mono-and bis-pyrazolyl-s-triazine ligands. *Polyhedron* **2020**, *187*, 114665. [[CrossRef](#)]

38. Soliman, S.M.; Lasri, J.; Haukka, M.; Elmarghany, A.; Al-Majid, A.M.; El-Faham, A.; Barakat, A. Synthesis, X-ray structure, Hirshfeld analysis, and DFT studies of a new Pd (II) complex with an anionic s-triazine NNO donor ligand. *J. Mol. Struct.* **2020**, *1217*, 128463. [CrossRef]
39. Al-Khodir, F.A.; Abumelha, H.; Al-Warhi, T.; Al-Issa, S.A. New platinum (IV) and palladium (II) transition metal complexes of s-triazine derivative: Synthesis, spectral, and anticancer agents studies. *BioMed Res. Int.* **2019**, *2019*, 9835745. [CrossRef]
40. Ismail, A.M.; El Sayed, S.A.; Butler, I.S.; Mostafa, S.I. New Palladium (II), Platinum (II) and Silver (I) complexes of 2-amino-4,6-dithio-1,3,5-triazine; synthesis, characterization and DNA binding properties. *J. Mol. Struct.* **2020**, *1200*, 127088. [CrossRef]
41. Barakat, A.; El-Senduny, F.F.; Almarhoon, Z.; Al-Rasheed, H.H.; Badria, F.A.; Al-Majid, A.M.; Ghabbour, H.A.; El-Faham, A. Synthesis, X-ray crystal structures, and preliminary antiproliferative activities of new s-triazine-hydroxybenzylidene hydrazone derivatives. *J. Chem.* **2019**, *2019*, 9403908. [CrossRef]
42. Altowyan, M.S.; Soliman, S.M.; Lasri, J.; Eltayeb, N.E.; Haukka, M.; Barakat, A.; El-Faham, A. A New Pt(II) Complex with Anionic s-Triazine Based NNO-Donor Ligand: Synthesis, X-ray Structure, Hirshfeld Analysis and DFT Studies. *Molecules* **2022**, *27*, 1628. [CrossRef]
43. Fathalla, E.M.; Abu-Youssef, M.A.M.; Sharaf, M.M.; El-Faham, A.; Barakat, A.; Badr, A.M.A.; Soliman, S.M.; Slawin, A.M.Z.; Woollins, J.D. Synthesis, Characterizations, Antitumor and Antimicrobial Evaluations of Novel Mn(II) and Cu(II) Complexes with NNN-tridentate s-Triazine-Schiff base Ligand. *Inorganica Chim. Acta* **2023**, *555*, 121586. [CrossRef]
44. Fathalla, E.M.; Abu-Youssef, M.A.M.; Sharaf, M.M.; El-Faham, A.; Barakat, A.; Haukka, M.; Soliman, S.M. Synthesis, X-ray Structure of Two Hexa-Coordinated Ni(II) Complexes with s-Triazine Hydrazine Schiff Base Ligand. *Inorganics* **2023**, *11*, 222. [CrossRef]
45. Bruker, A.X.S. *APEX2, Version 2014. 11-0*; Bruker: Madison, WI, USA, 2014.
46. Altomare, A.; Casciarano, G.; Giacovazzo, C.; Guagliardi, A.A. Completion and refinement of crystal structures with SIR92. *J. Appl. Crystallogr.* **1993**, *26*, 343–350. [CrossRef]
47. Sheldrick, G.M. Crystal structure refinement with SHELXL. *Acta Crystallogr. Sect. C Struct. Chem.* **2015**, *71*, 3–8. [CrossRef] [PubMed]
48. Farrugia, L.J. WinGX and ORTEP for Windows: An update. *J. Appl. Crystallogr.* **2012**, *45*, 849–854. [CrossRef]
49. Macrae, C.F.; Edgington, P.R.; McCabe, P.; Pidcock, E.; Shields, G.P.; Taylor, R.; Streek, J.V.D. Mercury: Visualization and analysis of crystal structures. *J. Appl. Crystallogr.* **2006**, *39*, 453–457. [CrossRef]
50. Turner, M.J.; McKinnon, J.J.; Wolff, S.K.; Grimwood, D.J.; Spackman, P.R.; Jayatilaka, D.; Spackman, M.A. Crystal Explorer17 (2017) University of Western Australia. Available online: <http://hirshfeldsurface.net> (accessed on 20 May 2019).
51. Frisch, M.J.; Trucks, G.W.; Schlegel, H.B.; Scuseria, G.E.; Robb, M.A.; Cheeseman, J.R.; Scalmani, G.; Barone, V.; Mennucci, B.; Petersson, G.A.; et al. *GAUSSIAN 09, revision A02*; Gaussian Inc.: Wallingford, CT, USA, 2009.
52. Glendening, E.D.; Reed, A.E.; Carpenter, J.E.; Weinhold, F. *NBO, version 3.1, CI*; University of Wisconsin: Madison, MI, USA, 1998.
53. Adamo, C.; Barone, V. Exchange functionals with improved long-range behavior and adiabatic connection methods without adjustable parameters: The mPW and mPW1PW models. *J. Chem. Phys.* **1998**, *108*, 664–675. [CrossRef]
54. Feller, D. The role of databases in support of computational chemistry calculations. *J. Comput. Chem.* **1996**, *17*, 1571–1586. [CrossRef]
55. Schuchardt, K.L.; Didier, B.T.; Elsethagen, T.; Sun, L.; Gurumoorthi, V.; Chase, J.; Li, J.; Windus, T.L. Basis set exchange: A community database for computational sciences. *J. Chem. Inf. Model.* **2007**, *47*, 1045–1052. [CrossRef]
56. Bader, R.F.W. *Atoms in Molecules: A Quantum Theory*; Oxford University Press: Oxford, UK, 1990.
57. Lu, T.; Chen, F. Multiwfn: A multifunctional wavefunction analyzer. *J. Comp. Chem.* **2012**, *33*, 580–592. [CrossRef] [PubMed]
58. Mosmann, T. Rapid colorimetric assay for cellular growth and survival: Application to proliferation and cytotoxicity assays. *J. Immunol. Methods* **1983**, *65*, 55–63. [CrossRef] [PubMed]
59. Khodair, A.I.; Bakare, S.B.; Awad, M.K.; Nafie, M.S. Design, synthesis, DFT, molecular modelling studies and biological evaluation of novel 3-substituted (E)-5-(arylidene)-1-methyl-2-thioxoimidazolidin-4-ones with potent cytotoxic activities against breast MCF-7, liver HepG2, and lung A549. *J. Mol. Struct.* **2021**, *1229*, 129805. [CrossRef]
60. Boraei, A.T.A.; Eltamany, E.H.; Ali, I.A.I.; Gebriel, S.M.; Nafie, M.S. Synthesis of new substituted pyridine derivatives as potent anti-liver cancer agents through apoptosis induction: In vitro, in vivo, and in silico integrated approaches. *Bioorg. Chem.* **2021**, *111*, 104877. [CrossRef]
61. ElZahabi, H.S.A.; Nafie, M.S.; Osman, D.; Elghazawy, N.H.; Soliman, D.H.; EL-Helby, A.A.H.; Arafa, R.K. Design, synthesis and evaluation of new quinazolin-4-one derivatives as apoptotic enhancers and autophagy inhibitors with potent antitumor activity. *Eur. J. Med. Chem.* **2021**, *222*, 113609. [CrossRef] [PubMed]
62. Kishk, S.M.; Kishk, R.M.; Yassen, A.S.; Nafie, M.S.; Nembr, N.A.; ElMasry, G.; Al-Rejaie, S.; Simons, C. Molecular insights into human transmembrane protease serine-2 (TMP2) inhibitors against SARS-CoV-2: Homology modelling, molecular dynamics, and docking studies. *Molecules* **2020**, *25*, 5007. [CrossRef]
63. Bohórquez, H.J.; Boyd, R.J.; Matta, C.F. Molecular model with quantum mechanical bonding information. *J. Phys. Chem. A* **2011**, *115*, 12991–12997. [CrossRef] [PubMed]
64. Bader, R.F. A quantum theory of molecular structure and its applications. *Chem. Rev.* **1991**, *91*, 893–928. [CrossRef]
65. Bhadane, S.A.; Lande, D.N.; Gejji, S.P. Understanding binding of cyano-adamantyl derivatives to pillar [6] arene macrocycle from density functional theory. *J. Phys. Chem. A* **2016**, *120*, 8738–8749. [CrossRef]



66. Marana, N.L.; Casassa, S.M.; Sambrano, J.R. Adsorption of NH<sub>3</sub> with different coverages on single-walled ZnO nanotube: DFT and QTAIM study. *J. Phys. Chem. C* **2017**, *121*, 8109–8119. [[CrossRef](#)]
67. Akman, F.; Issaoui, N.; Kazachenko, A.S. Intermolecular hydrogen bond interactions in the thiourea/water complexes (Thio-(H<sub>2</sub>O)<sub>n</sub>)(n = 1, . . . , 5): X-ray, DFT, NBO, AIM, and RDG analyses. *J. Mol. Model.* **2020**, *26*, 161. [[CrossRef](#)] [[PubMed](#)]
68. Venkataramanan, N.S.; Suvitha, A.; Kawazoe, Y. Unravelling the nature of binding of cubane and substituted cubanes within cucurbiturils: A DFT and NCI study. *J. Mol. Liq.* **2018**, *260*, 18–29. [[CrossRef](#)]
69. Nimmermark, A.; Öhrström, L.; Reedijk, J. Metal-ligand bond lengths and strengths: Are they correlated? A detailed CSD analysis. *J. Z. Krist.* **2013**, *228*, 311–317. [[CrossRef](#)]
70. Reed, A.E.; Weinstock, R.B.; Weinhold, F. Natural population analysis. *J. Chem. Phys.* **1985**, *83*, 735–746. [[CrossRef](#)]
71. Fernández-Delgado, E.; Estirado, S.; Rodríguez, A.B.; Luna-Giles, F.; Viñuelas-Zahínos, E.; Espino, J.; Pariente, J.A. Cytotoxic Effects of New Palladium(II) Complexes with Thiazine or Thiazoline Derivative Ligands in Tumor Cell Lines. *Pharmaceutics* **2023**, *15*, 696. [[CrossRef](#)]
72. Sun, Y.; Sun, D.; Yu, W.; Zhu, M.; Ding, F.; Liu, Y.; Gao, E.; Wang, S.; Xiong, G.; Dragutan, I.; et al. Synthesis, Characterization, Interaction with DNA and Cytotoxicity of Pd(II) and Pt(II) Complexes Containing Pyridine Carboxylic Acid Ligands. *Dalton Trans.* **2013**, *42*, 3957–3967. [[CrossRef](#)]
73. Masuda, H.; Zhang, D.; Bartholomeusz, C.; Doihara, H.; Hortobagyi, G.N.; Ueno, N.T. Role of Epidermal Growth Factor Receptor in Breast Cancer. *Breast Cancer Res. Treat.* **2012**, *136*, 331–345. [[CrossRef](#)]
74. Ali, A.; Banerjee, S.; Kamaal, S.; Usman, M.; Das, N.; Afzal, M.; Alarifi, A.; Sepay, N.; Roy, P.; Ahmad, M. Ligand Substituent Effect on the Cytotoxicity Activity of Two New Copper(II) Complexes Bearing 8-Hydroxyquinoline Derivatives: Validated by MTT Assay and Apoptosis in MCF-7 Cancer Cell Line (Human Breast Cancer). *RSC Adv.* **2021**, *11*, 14362–14373. [[CrossRef](#)]

**Disclaimer/Publisher's Note:** The statements, opinions and data contained in all publications are solely those of the individual author(s) and contributor(s) and not of MDPI and/or the editor(s). MDPI and/or the editor(s) disclaim responsibility for any injury to people or property resulting from any ideas, methods, instructions or products referred to in the content.